Hindawi
Scientific Programming
Volume 2021, Article ID 4505147, 10 pages
https://doi.org/10.1155/2021/4505147

Research Article

Convolutional Neural Network Optimization Algorithm-Based Magnetic Resonance Imaging in Analysis of Chronic Pain Caused by the Myofascial Trigger Point

Xin Jin,[1] **Lei Fan**,[2] **and Yongling Yao**[1]

[1]*Department of Pain, Xiangyang First People's Hospital, Xiangyang, Hubei 441000, China*
[2]*Department of Urology Surgery, Xiangyang First People's Hospital, Xiangyang, Hubei 441000, China*

Correspondence should be addressed to Yongling Yao; 17127915@bjtu.edu.cn

Received 8 July 2021; Revised 14 August 2021; Accepted 16 August 2021; Published 7 September 2021

Academic Editor: Gustavo Ramirez

This study was to explore the value of magnetic resonance imaging (MRI) technology processed by convolutional neural network (CNN) optimization algorithms in the clinical research of patients with chronic pain caused by myofascial trigger points (MTrPs). Firstly, referring to the traditional iterative algorithm, this study iterated the convolution network and data consistency layer as a whole for several times, which increased the fitting ability of the data consistency layer and network. When it was applied to magnetic resonance examination, it could be concluded that the effect of its reconstruction method was better than the traditional convolution neural network without the data consistency layer. The image edge was clear, and the restoration effect of details was better. 100 patients with chronic neck pain caused by MTrP were collected and divided into an ultrasound treatment group and a local anesthetic drug injection group, with 50 cases in each group. In addition, 50 healthy volunteers were selected. After clinical treatment, the results showed that, after 3 weeks of treatment, the visual analog score (VAS) and the pain rating index (PRI) of the injection group were 3.16 ± 1.14 points and 4.92 ± 1.26 points, respectively; the present pain intensity (PPI) score was 2.06 ± 0.85 points, and the number of pain days per month was 7.73 ± 1.15. After 1 month of treatment, the VSA and PRI of the injection group were 1.24 ± 0.89 and 1.31 ± 0.97, respectively; the PPI score was 1.34 ± 0.65, and the number of pain days per month was 5.34 ± 0.98. In addition, there were 38 cases reaching the level of clinical cure, accounting for 76%. Therefore, all indicators in the injection group were better than those in the ultrasound treatment group, and the differences were statistically significant ($P < 0.05$). The results of MRI examination showed that compared with the healthy control group, patients with chronic pain caused by the myofascial trigger point had reduced axial kurtosis (AK), mean kurtosis (MK), and radial kurtosis (RK) in multiple brain areas such as the right parahippocampal gyrus and the right medial prefrontal cortex. In short, chronic pain caused by the trigger point of the myofascial membrane would affect the microstructure of the gray matter of the patient's brain. In clinical treatment, the efficacy of local anesthetic injection was better than ultrasound therapy.

1. Introduction

Myofascial pain syndrome (MPS) is a group of clinically common pain syndromes, mostly in middle-aged and elderly people, often caused by the activation of myofascial pain trigger points (MTrP) on the skeletal muscle [1, 2]. In 1942, the American professor Janet Travel firstly discovered that the trigger point of myofascial pain is caused by the formation of skeletal muscle tension bands for some reason, causing long-term muscle imbalance in muscles, leading to a series of myofascial pain syndromes [3]. Current studies believe that the lesion of myofascial pain is not in the myofascial, but in the motor endplate of skeletal muscle. Long-term myofascial pain will lead to the facilitation change of spinal cord level. The reasons for the formation of pain trigger points are not single, including skeletal muscle system trauma, various inflammation, insufficient or excessive exercise, and hormone level changes. The main clinical manifestations are myogenic pain, stretch pain, and adhesion contracture caused by local myofascial injury. It

has the characteristics of delayed onset, long course of disease, and repetitive attacks. In severe cases, it can also lead to restricted activities and even loss of work ability [4, 5]. This chronic pain has a great impact on the quality of sleep, work, and life of patients.

Regarding the pathogenesis of the trigger point, there is no clear conclusion in the medical field. However, it is generally believed that the dysfunctional endplate is the main factor in the formation of the trigger point. When the body is in a pathological state, the neurotransmitter acetylcholine in the motor endplate, which is distributed in the skeletal muscle and formed by the axon terminals of motor neurons and skeletal muscle fibers, will be released continuously for a long time. Binding to the receptors on the muscle cell membrane will cause the skeletal muscle fibers to contract continuously for a long time. In this way, nodules will gradually form, the local energy of the body will be consumed a lot, and the local blood circulation will be inhibited, resulting in a lack of adenosine triphosphate supply [6–8]. While the nodules contract, they can also stimulate the cells to release interleukin-6, capsaicin, bradykinin, and other pain-causing substances, which intensifies the pain of skeletal muscles. These substances will also lower the activation threshold of nerves, leading to activation and sensitization of peripheral nerve endings and motor nerves, activating the secondary nerves, and leading to central sensitization [9–11]. When MTrP are properly treated clinically, local pain and involved pain can be more effectively reduced, perhaps due to the reduction of nociceptive stimulus signals introduced into the spinal dorsal horn neurons, which controls the spread of pain and central sensitization. If central sensitization can be reversed in this way, the clinical treatment of chronic pain caused by MTrP will have another possibility.

Many studies have proved that the brain structure of patients with chronic pain would change to a certain extent. The connection between brain regions of some patients with chronic pain is stronger or weaker than that of healthy people, and their abilities of learning, cognition, and memory will be affected. Magnetic resonance imaging (MRI) is a technology that uses the resonance of atomic nuclei in a strong magnetic field to generate signals for image reconstruction. It is widely used in clinic because of its noninvasive, multiplanar parameter imaging, no ionizing radiation, high spatial resolution, and high repeatability. It is also of great value in studying the changes of brain structure and function in the field of pain, forming a modern medical model and improving human health [12, 13]. However, its clinical application has certain limitations, mainly because the MRI imaging speed is slow, and the image quality is easily affected by the subject's physiological and involuntary movements, which will produce images with artifacts and noise. The traditional MRI image optimization methods are computationally complex and do not have good real-time performance. CNN is a typical representative of feedforward neural network, especially in image processing, including image classification, target detection, and image segmentation. Therefore, a data consistency layer was added on the basis of convolutional neural networks (CNN) in this study. With reference to the traditional iterative algorithm, the CNN and the data consistency layer as a whole were iterated several times to increase the fitting ability of the network [14, 15] to achieve the optimization of MRI images.

In this study, the CNN optimization algorithm was used in MRI technology to explore its clinical analysis value in 100 patients with chronic pain caused by MTrP and to provide more reference for the clinical treatment and research of MTrP.

2. Materials and Methods

2.1. Research Objects. 100 patients with chronic neck pain caused by MTrP in the hospital from April 2018 to April 2020 were selected as research objects. They were aged 20–50 years and were randomly divided into an ultrasound treatment group and a drug injection group, with 50 cases in each group. The inclusion criteria were defined as follows: patients with at least one active muscle trigger point on both trapezius muscles; patients with pain history ≥3 months; patients with pain or radiating pain by puncturing the trigger point; patients with VAS ≥5 points; patients with limited activity of skeletal muscle; patients with insufficiency of sleep or increased pain in the state of tension; patients whose MRI examination showed cervical spine and spine without deformity and nerve root compression; and patients with complete clinical data and who could cooperate with examination and treatment. The exclusion criteria were defined as follows: patients with cervical spondylosis, cervical vertebra deformity, or nerve root compression pain; patients with a history of sprains or trauma in the neck; patients with a history of trapezius or neck surgery; pregnant and lactating women; patients with other serious organ diseases; patients with brain parenchymal disease; patients with metal in the body or with pacemaker; and patients with poor compliance or incomplete clinical data. In addition, 50 healthy volunteers in the same age range who underwent physical examination in the hospital during the same period were selected in the control group. The inclusion criteria were defined as follows: patients with no obvious signs of pain throughout the body and patients with no activity or latent MTrP in the bilateral trapezius muscles. The exclusion criteria were the same as above. All patients stopped taking aniline drugs and anti-inflammatory drugs that did not contain steroids 3 days before the start of the experiment. Participants and their family members had been notified of the experiment related matters, and they had all signed the informed consent forms.

2.2. MRI Examination. After routine preparations, all patients with myofascial pain and healthy participants were placed in a supine position with the head advanced, the upper limbs placed on both sides of the body, and the earplugs were inserted into special earplugs (Shanghai Linghe Protective Technology Co., Ltd.). In addition, they were advised not to move. The equipment adopted Magnetom Avanto 1.5 T superconducting high field intensity MRI whole body scanner, scanning the whole brain in

sagittal position. The parameters were set as follows: time of repetition (TR)/time of echo (TE) was 7.8/3, field of view (FOV) was 240 mm × 240 mm, the scanning thickness was roughly 5 mm, the layer distance was 1.5 mm, and the number of layers was 20. The scanning parameters of diffusion kurtosis imaging (DKI) were defined as follows: TR/TE was 10000/99.3, the FOV was 240 mm × 240 mm, the layer thickness was 5 mm, the layer distance was 0 mm, and the number of layers was 30.

2.3. Optimization Algorithm Based on the CNN. The brain image data processing software was used to correct the MRI image, and the kurtosis evaluation software was to evaluate the mean kurtosis (MK), axial kurtosis (AK), and radial kurtosis (RK) measured. The image was optimized using CNN.

Firstly, the basic principles of the CNN were introduced. It was supposed that $x \in A^N$ was a column containing s elements after expansion, which was the composite signal of the real signal and the imaginary signal of the MRI image. $S = S_x S_y$, $y = A^K (K \le F)$ was the observation object, and $f \in A^K$ represented the Gaussian white noise generated by the signal coordinate system in the frequency. The imaging process of MRI images is shown in

$$y = G_n x + f. \tag{1}$$

In the equation above, $G_n \in A^{K \times F}$ referred to the undersampling operator, $(G_n = KG)$, and the operation of this operator consisted of two steps. Firstly, the MRI image signal was transferred to the signal coordinate domain using $G \in A^{F \times F}$, and then the signal was undersampled in the coordinate domain using the coordinate domain undersampling template $K \in A^{K \times F}$. The sorted storage structures corresponding to all sampling points were collected and set as a set Ω. The entire process of obtaining the initial MRI image signal x from the observation signal y was called MRI image optimization.

Due to the atypicality of G_n, the obtained solution was not unique and the instability was high if it is directly reversed. Therefore, in order to obtain high stability and the only solution, it was also necessary to use the experience and historical data obtained by the image itself before the experiment of obtaining the sample to solve the negation here. A classic and common method was adopted, which meant to add a regular term and obtain the unique solution by delimiting the category of the solution. The equation is given as follows:

$$\min_x \varsigma(x) + \lambda \left\| y - G_n x \right\|_2^2. \tag{2}$$

In the equation above, ς referred to the regular term corresponding to x, and $\lambda \in \Psi$ was the adjustment factor. According to the interference degree of Gaussian white noise, the signal coordinate domain was adjusted to standardize the unity of MRI and observation signals. In deep learning MRI image optimization, the expression of the learned image samples by the convolutional neural network was relatively abstract, so the abstract expression learned by the trained convolutional neural network can be used as a test for obtaining the experience and historical data obtained before obtaining the samples in the MRI image, so that it could be added to the optimization equation as a regular term as follows:

$$\min_x \left\| x - g_{cnn}(x_n|\theta) \right\|_2^2 + \lambda \left\| G_n x - y \right\|_2^2. \tag{3}$$

In (3), θ was a large number of adjustable parameters included in the convolutional neural network, and g_{cm} represented the forward propagation method of the convolutional neural network. The mixed superimposed image x_n obtained by the conversion of the observation signal y is the input of the convolutional neural network to get the optimized image.

In the above equation, x_n was obtained under the undersampling operation, which did not conform to the sampling principle. The image signal had aliasing in the time relationship, so the optimization of the CNN can also be regarded as a process of time-domain antialiasing; then the overall optimized image of the network can be expressed as follows:

$$x_{cnn} = g_{cnn}(x_n|\theta, \lambda, \Omega). \tag{4}$$

Because the CNN used some coordinate domain signal sampling points of the real MRI image to complete the optimization, the values of these sampling points should be consistent before and after optimization. However, the optimization process was better than the operation in the coordinate domain, and there was a certain difference between the MRI image optimized by the CNN and the real image. In order to improve the accuracy of optimization, how to determine the value of the sampling point requires the application of two parts: the initial value and the CNN optimization value. Therefore, the optimization of MRI images was performed by CNN optimization and data consistent operation.

When a CNN was trained, the input training data pair Ψ: $(x_n, x_{\text{gnd}}), x_{\text{gnd}}$ represented the real image, and the network parameter values were adjusted through the cost function to obtain the most optimized network.

$$\sigma(\theta) = \sum_{(x_n, x_{\text{gnd}}) \in \Psi} \vartheta\left(x_{\text{gnd}}, x_{cnn}\right). \tag{5}$$

In (5), ϑ was the cost function. In this study, the cost of the mean square error (MSE) needed to be considered, which was expressed as follows:

$$\vartheta\left(x_{\text{gnd}}, x_{cnn}\right) = \left\| x_{\text{gnd}} - x_{cnn} \right\|_2^2. \tag{6}$$

Then, the least squares method was adopted to find the extreme value of the function:

$$\left(x - g_{cnn}(x_n|\theta)\right) + \lambda G_n^M \left(G_n x - y\right) = 0. \tag{7}$$

Equation (8) could be obtained by simplifying the above equation:

$$\left(J + \lambda G_n^M G_n\right)x = g_{cnn}\left(x_n|\theta\right) + \lambda G_n^M y. \tag{8}$$

All the data were transformed to the coordinate domain and then calculated:

$$\left(J + \lambda G G_n^M\right)Gx = Gg_{cnn}\left(x|0\right) + \lambda G G_n^M y. \tag{9}$$

The following equation can be obtained by writing the above equation in the form of factor-by-factor calculation:

$$\begin{aligned} Z_{\text{rec}}(l) &= Z_{cnn}(l) \quad \text{if } l \notin \Omega, \\ Z_{\text{rec}}(l) &= \frac{Z_{cnn}(l) + \lambda Z_0(l)}{1+\lambda} \quad \text{if } l \in \Omega. \end{aligned} \tag{10}$$

In the above two equations, Z_{rec} referred to the optimized image of the final signal coordinate domain, and the optimized image of the entire network $x_{\text{rec}} = G^M l_{\text{rec}}$ could be obtained after transformation. The above equation can be used as a popular explanation: for the image of the undersampled signal coordinate domain, if point l was not sampled, which was to optimize the value of the corresponding orientation of the image, the CNN could be applied to optimize the value; if point l was the sampling point, $l \in \Omega$, and the value of the orientation corresponding to the optimized image was the linear set of the CNN optimization value and the initial sampling value.

Although the CNN can fit some complex and difficult images in more depth, it had to require a certain amount of data in the sample set; otherwise, overfitting would often occur. It usually takes a long time to train the network, and the parameters need to be adjusted carefully. In this study, different sampling templates of the same multiple were adopted for the training sample set, and a fixed template was applied for the test set that needs to be undersampled. The peak signal-to-noise ratio (SNR), root mean square error (RMSE), and structural similarity (SIM) were used to express the optimization results. The equations were as follows:

$$\text{PSNR} = 10 \times \log_{10}\frac{\max}{\sqrt{\text{MSE}}}. \tag{11}$$

In the equation above, max represented the maximum pixel value in the initial image and MSE was the mean square error.

$$\text{NMSE} = \sqrt{\frac{\|x-y\|^2\ G}{\|x\|_G^2}}, \tag{12}$$

$$\text{SSIM}(x,y) = \frac{\left(2\phi_x\phi_x + p_1\right)\left(2\eta_{xy} + p_2\right)}{\left(\phi_x^2 + \phi_x^2 + p_1\right)\left(\eta_x^2 + \eta_x^2 + p_1\right)}. \tag{13}$$

In (12) and (13), x and y represented the initial image and the optimized result; ϕ_x, ϕ_y and η_x^2, η_y^2 represented the average value and variance of each of x and y; η_{xy} referred to the standard deviation of x and y; and p_1 and p_2 were constants used to maintain stability. The value range of structural similarity was [−1, 1]. When the images before and after optimization were the same, the value of SSIM was 1.

2.4. Ultrasound Therapy. LCA300 ultrasonic therapy instrument (Chattanooga, USA) with standard 8-channel cranial coil was applied, the frequency was set to 3.3 MHz, the pulse duration was 5 ms, and amplitude was 0–3 W/cm2. Patients in the ultrasound group went to the treatment bed and took a lateral position to fully expose the trigger point of the trapezius muscle. The operator held the ultrasound head and performs myofascial pulse radio frequency on the key MTrP of the patient's neck for 20–30 minutes, with 3-4 times a week. During the treatment, the patient's own condition and response had to be observed, and the intensity of the ultrasound pulse was adjusted according to the patient's tolerance.

2.5. Drug Injection Therapy. The operator stood behind the patient in the injection group, asked the patient to ride, sit upside down on the back chair, sit upside down at the desk, put the forehead on the arm, and tilt the head to the unaffected side to confirm the position of the trigger point with the index finger of the left hand, which was marked. After routine disinfection of the drapes, 5 mL of 2% lidocaine (Sihuan Pharmaceutical Co., Ltd.) was diluted to 20 mL with 0.9% sodium chloride injection (Sinopharm Group Rongsheng Pharmaceutical Co., Ltd.) and then injected with No. 5 needle (Shanghai Rui Bosai Biotechnology Co., Ltd.). The skin at the trigger point was fixed with the index finger of the left hand and injected carefully with the syringe in the right hand until the patient complained that he feels the trigger point. The fixed needle was slowly injected with liquid. After the injection was completed, the needle was pulled out, pressed with a sterile cotton ball, and fixed with tape. During the injection process, it had to pay close attention to the patient's own condition and reaction, stay in the hospital for observation for at least half an hour after the injection, and leave the hospital if there is no abnormality. Most patients only needed one injection, and a few patients needed 2–4 injections. It was better to keep more than 1 week between two injections.

2.6. VAS Score. The VAS method was used for pain assessment, which was widely used in clinical practice. The basic method was to use a moving ruler with the length of about 10 cm, with 10 scales on one side and "0″ and "10″ at both ends. 0 points meant no pain, and 10 points meant the most severe pain that was unbearable (as shown in Figure 1).

2.7. PRI Score. Pain rating index (PRI) was composed of 15 expression words, 11 of which were related to sensory expression and 4 were related to emotional expression. Each expression was followed by a grade of intensity. The sum of the scores of 15 options was the total pain score (as shown in Table 1).

2.8. PPI Score. The present pain intensity (PPI) was to allow the patient to mark after the corresponding score based on the current subjective feelings (shown in Table 2).

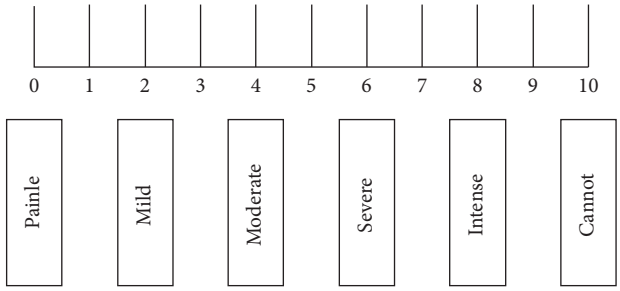

Figure 1: VAS score.

Table 1: PRI.

A. Feeling	Painless	Mild	Medium	Severe
Throbbing pain	0 scores	1 score	2 scores	3 scores
Tingling	0 scores	1 score	2 scores	3 scores
Knife cut	0 scores	1 score	2 scores	3 scores
Sharp pain	0 scores	1 score	2 scores	3 scores
Cramping pain	0 scores	1 score	2 scores	3 scores
Bite	0 scores	1 score	2 scores	3 scores
Burning pain	0 scores	1 score	2 scores	3 scores
Sore	0 scores	1 score	2 scores	3 scores
Falling pain	0 scores	1 score	2 scores	3 scores
Tenderness	0 scores	1 score	2 scores	3 scores
Cleavage pain	0 scores	1 score	2 scores	3 scores
B. Emotion				
Exhaustion	0 scores	1 score	2 scores	3 scores
Sickness	0 scores	1 score	2 scores	3 scores
Sense of fear	0 scores	1 score	2 scores	3 scores
Sense of punishment	0 scores	1 score	2 scores	3 scores

Table 2: PPI score.

Score	Pain intensity
0	Painless
1	Mild
2	Uncomfortable
3	Pain and irritability
4	Terrible
5	Extreme pain

2.9. Statistical Analysis. After the database was established, statistical analysis was performed using SPSS 24.0 software. Measurement data was expressed as mean ± standard deviation ($\bar{x} \pm s$). The comparison of multisample means used a completely randomized design of variance analysis. The data at each time point adopted the repeated measures analysis of variance model, and the count data analysis was performed using the χ^2 test. $P < 0.05$ indicated that the difference was statistically significant.

3. Results

3.1. Comparison on the General Data of Patients. 100 patients with chronic pain in the trapezius muscle caused by MTrP were enrolled in this study. They were divided into an ultrasound treatment group of 50 cases, a drug injection group of 50 cases, and a healthy control group of 50 cases. As shown in Table 3, the three groups of participants had no obvious differences in general clinical data such as gender distribution, age, course of disease, height, weight, and body mass index (BMI), which were not statistically significant ($P > 0.05$).

3.2. Comparison of Pain Scores between the Ultrasound Group and Injection Group before Treatment. As illustrated in Table 4, there was no obvious difference in the VAS score, PRI score, and PPI score between the ultrasound treatment group and the drug injection group of patients before treatment ($P > 0.05$), and they can be compared.

3.3. Comparison of the Pain Days per Month before Treatment between the Ultrasound Group and the Injection Group. As revealed in Figure 2, there was no statistically visible difference in the number of pain days per month between the ultrasound treatment group and the drug injection group before treatment ($P > 0.05$), and they can be compared.

3.4. Comparison of VAS Scores between the Ultrasound Group and Injection Group after Treatment. As given in Figure 3, patients in the ultrasound group had a VAS score of 5.27 ± 1.12 scores, while those in the injection group had a score of 4.88 ± 1.06 after 1 week of treatment, showing no statistically significant difference ($P > 0.05$). After 3 weeks of treatment, the VAS score of the ultrasound group was 3.88 ± 1.25 points, and that in the injection group was 3.16 ± 1.14 points. After 1 month of treatment, the VAS score of patients in the ultrasound group was 1.75 ± 0.98 points, that of the injection group was 1.24 ± 0.89 points, and the difference was statistically significant ($P < 0.05$).

3.5. Comparison of PRI Scores between the Ultrasound Group and Injection Group after Treatment. As shown in Figure 4, patients in the ultrasound group had a PRI score of 11.46 ± 1.87 points, while those in the injection group had a score of 11.35 ± 1.74 points after 1 week of treatment, and the difference was not statistically significant ($P > 0.05$). After 3 weeks of treatment, the PRI score of the ultrasound group was 5.68 ± 1.53 scores, and the injection group was 4.92 ± 1.26 scores. After 1 month of treatment, the PRI score of patients in the ultrasound group was 2.14 ± 1.01 score, the score of the injection group was 1.31 ± 0.97, and the difference was statistically significant ($P < 0.05$).

3.6. Comparison of PPI Scores between the Ultrasound Group and Injection Group after Treatment. As revealed in Figure 5, patients in the ultrasound group had a PPI score of 3.87 ± 1.14 points, while those in the injection group were 3.79 ± 1.08 points after 1 week of treatment, the difference was not statistically significant ($P > 0.05$). After 3 weeks of treatment, the PRI score of the ultrasound group was 2.54 ± 1.2 scores, and the injection group was 2.06 ± 0.85 scores; after 1 month of treatment, the PRI score of the

Table 3: Comparison on the general data of patients.

Baseline data	Group	$\bar{x} \pm s$	P
Age (years old)	Ultrasound group	36.83 ± 3.72	0.849
	Drug group	37.19 ± 3.66	
	Healthy group	38.2 ± 4.11	
Male (people)	Ultrasound group	27	0.733
	Drug group	28	
	Healthy group	25	
Course (month)	Ultrasound group	12.37 ± 5.6	0.751
	Drug group	11.82 ± 4.9	
	Healthy group	0	
Height (cm)	Ultrasound group	167.82 ± 7.93	0.323
	Drug group	168.54 ± 7.86	
	Healthy group	169.03 ± 7.21	
Weight (kg)	Ultrasound group	67.24 ± 9.85	0.258
	Drug group	66.53 ± 8.94	
	Healthy group	67.11 ± 9.12	

Table 4: Comparison of pain scores between the ultrasound group and injection group before treatment.

Rating scale	Group	$\bar{x} \pm s$	P
VAS (score)	Ultrasound group	5.7 ± 1.38	0.783
	Drug group	5.5 ± 1.42	
PRI (score)	Ultrasound group	15.58 ± 2.81	
	Drug group	15.83 ± 2.76	
PPI (score)	Ultrasound group	4.18 ± 1.02	
	Drug group	4.21 ± 1.05	

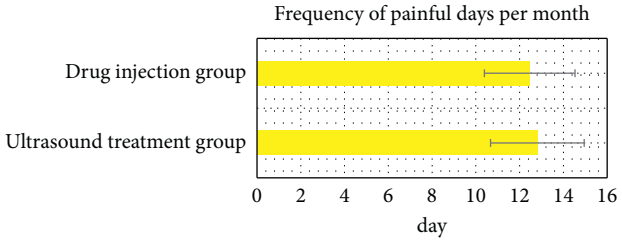

Figure 2: Comparison of the pain days per month before treatment between the ultrasound group and the injection group.

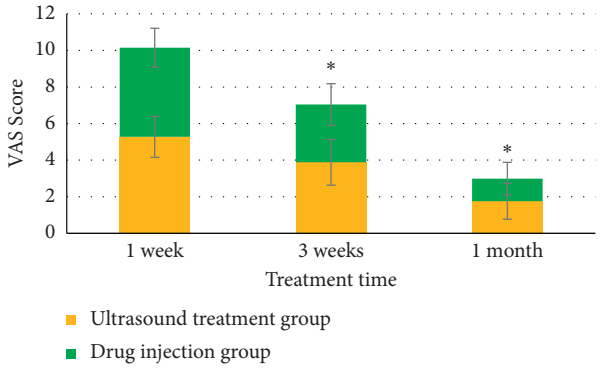

Figure 3: Comparison of VAS scores between the ultrasound group and injection group after treatment. * indicated that the statistical difference was visible between the VAS score 3 weeks after the treatment and 1 month after the treatment ($P < 0.05$).

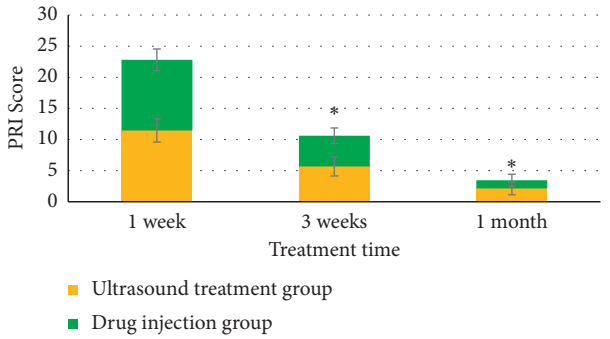

Figure 4: Comparison of PRI scores between the ultrasound group and injection group after treatment. * indicated that the statistical difference was visible between the PRI score 3 weeks after the treatment and 1 month after the treatment ($P < 0.05$).

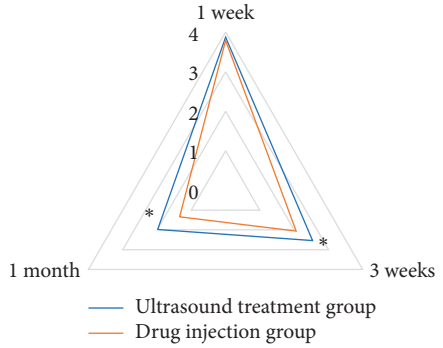

Figure 5: Comparison of PPI scores between the ultrasound group and injection group after treatment. * indicated that the statistical difference was visible between the PPI score 3 weeks after the treatment and 1 month after the treatment ($P < 0.05$).

ultrasound group was 1.98 ± 0.72 scores, while the injection group was 1.34 ± 0.65 scores, and the difference was statistically significant ($P < 0.05$).

3.7. Comparison of the Pain Days per Month after Treatment in the Ultrasound Group and the Injection Group. As illustrated in Figure 6, patients in the ultrasound group had 10.79 ± 1.93 pain days per month, while those in the injection group was 10.62 ± 1.85 days, and the difference was not statistically significant ($P > 0.05$). After 3 weeks of treatment, the number of painful days per month in the ultrasound group was 8.34 ± 1.21 days and that in the injection group was 7.73 ± 1.15 days; after 1 month of treatment, the number of pain days per month in the ultrasound group was 6.88 ± 1.02 days, while that in the injection group was 5.34 ± 0.98 days, and the difference was statistically significant ($P < 0.05$).

3.8. Comparison of the Effects of the Ultrasound Group and Injection Group after Treatment. As illustrated in Figure 7, there were 27 patients in the ultrasound treatment group that achieved a clinical cure effect (accounting for 54%), and there were 38 patients in the drug injection treatment group that achieved a clinical cure effect (accounting for 76%). It can be known that the difference was statistically significant ($P < 0.05$).

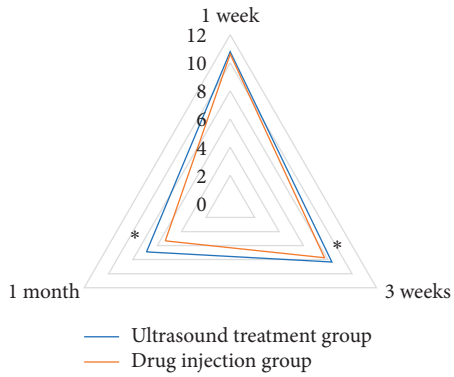

Figure 6: Comparison of the pain days per month after treatment in the ultrasound group and the injection group. * indicated that the statistical difference was visible between the pain days per month 3 weeks after the treatment and 1 month after the treatment ($P < 0.05$).

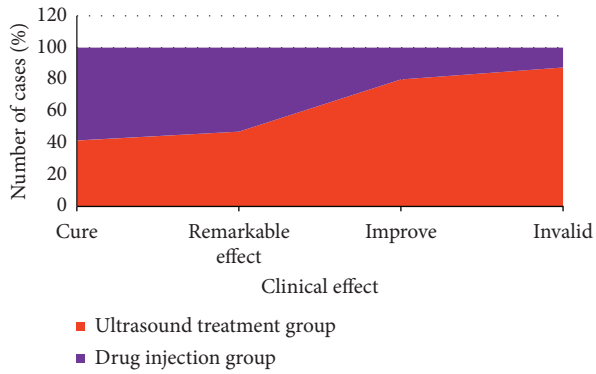

Figure 7: Comparison of the effects of the ultrasound group and injection group after treatment. * indicated that the statistical difference was visible between the number of clinically cured patients 3 weeks after the treatment and 1 month after the treatment ($P < 0.05$).

3.9. Comparison on MRI Images before and after CNN Optimization. There was a patient, male, 42 years old, who suffered from intermittent headaches for more than ten years, which worsened after lowering his head and neck exercises and worsened after staying up late. During the routine MRI examination, the imaging speed was slow, the image display was not clear, and there was extra interference noise due to the old equipment and other reasons, which brought some difficulties to the diagnosis and judgment of the disease. After the CNN optimization algorithm was applied to the MRI imaging technology, the obtained image was clear and no unnecessary noise was seen (as shown in Figure 8).

3.10. Brain Regions Where the AK Value of Patients with Chronic Pain Caused by MTrP Decreased. Compared with participants in the healthy control group, patients with chronic pain caused by MTrP had decreased AK in the right parahippocampal gyrus, right medial prefrontal cortex, and right inferior frontal gyrus (as shown in Table 5 and Figure 9).

3.11. Brain Regions Where the MK Value of Patients with Chronic Pain Caused by MTrP Decreased. Compared with participants in the healthy control group, patients with chronic pain caused by MTrP had decreased MK in the left parahippocampal gyrus, right middle temporal gyrus, and right anterior cingulate cortex, as shown in Table 6 and Figure 10.

3.12. The Brain Area Where the RK Value of Patients with Chronic Pain Caused by MTrP Decreased. Compared with the participants in the healthy control group, the RK of the left lingual gyrus, left middle temporal gyrus, and right precuneus of patients with chronic pain caused by MTrP decreased, as shown in Table 7 and Figure 11.

4. Discussion

MPS is a common and frequently occurring disease, and it can be summarized as local pain syndrome characterized by MTrP and tension zone [16]. In 1986, the International Society for Pain Research put forward the concept of MPS: pathogenic factors invade the fibrous tissues of the neck, shoulders, waist, back, and other parts, causing tissue damage and aseptic inflammation and resulting in extensive muscle pain and spasm in this part. MTrP is an important part of the diagnosis and treatment of MPS, as well as an important etiological mechanism of MPS [17, 18]. The chronic pain caused by the trigger point starts from the nociceptors, and some chemical stimuli such as muscle metabolites and pain-causing substances can also activate the nociceptors [4, 19] and ultimately lead to central sensitization. This chronic pain can induce changes in the microstructure of the brain. Based on the MRI technology, the changes in the brain microstructure of patients with chronic pain caused by MTrP can be explored.

Compared with traditional medical imaging technology, MRI system shows many advantages, such as multiple available imaging parameters, high imaging contrast, direct tomographic imaging in any orientation, and no ionizing radiation [20], so it is widely used in clinical practice. However, the imaging speed of MRI is very slow due to its imaging principle, the entire inspection takes tens of minutes, and its images are easily affected by motion, resulting in artifacts and Gaussian noise, which affect the quality of the image. In recent years, CNN have shown great potential in natural image processing. Therefore, the original MRI image was undersampled based on the CNN optimization algorithm to increase the imaging speed, while removing redundant interference factors [21], so as to obtain higher quality MRI images.

100 patients with chronic neck pain caused by MTrP were selected and rolled into an ultrasound treatment group and a local anesthetic drug injection group, with 50 cases in each group. In addition, 50 healthy volunteers were selected as the control group. All participants received MRI examinations. The image was processed by a CNN optimization algorithm. After clinical treatment, the results showed that, after 3 weeks and 1 month of treatment, the VAS score, PRI score, PPI score, monthly pain days, and the number of cases

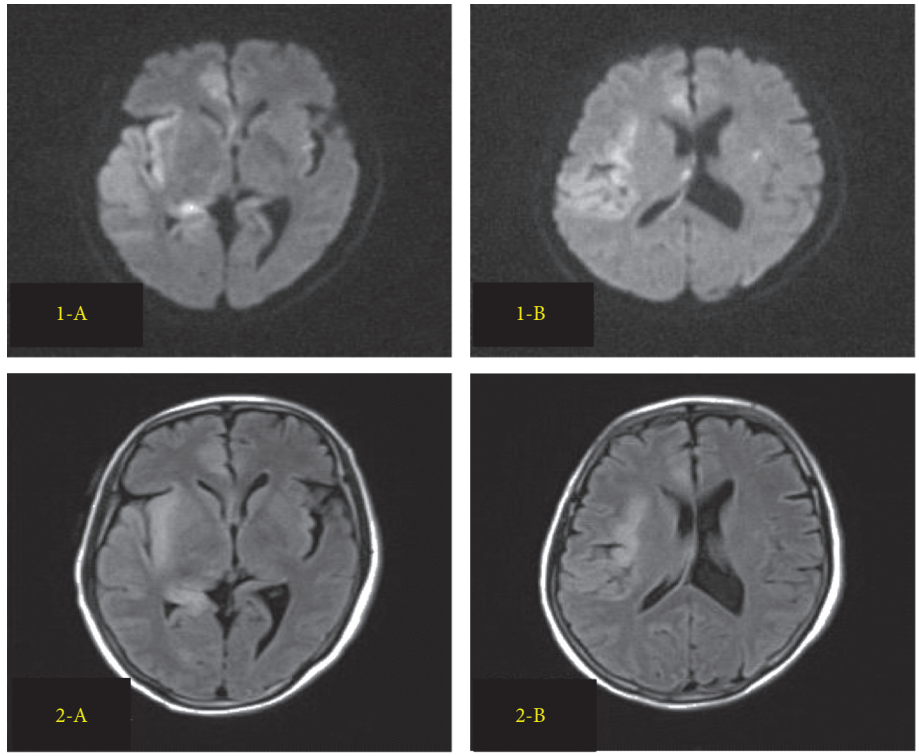

Figure 8: 1-A and 1-B were the original MRI images and 2-A and 2-B were the clear MRI images obtained after applying the CNN optimization algorithm.

Table 5: Brain regions where the AK value of patients with chronic pain caused by MTrP decreased.

Area of interest (AOI)	Peak MNI coordinate			Cluster voxel number	*T* value
	X	*Y*	*Z*		
Right parahippocampal gyrus	20	−40	−14	503	−3.95
Right medial prefrontal cortex	5	52	21	930	−4.03
Right inferior frontal gyrus	15	15	15	1008	−3.66

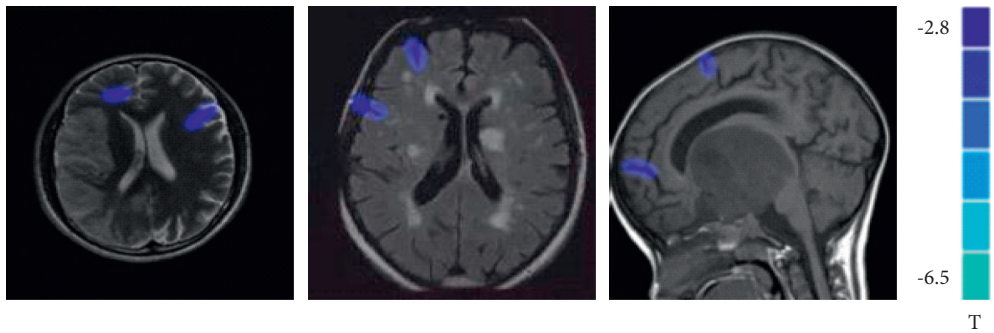

Figure 9: Brain regions where the AK value of patients with chronic pain caused by MTrP decreased. Blue area represented the brain area with reduced AK ($P < 0.05$). The colored bars represented the *T* value. The left and right side of the figure represented the right and left side of the anatomy, respectively.

cured in the injection group were better than those in the ultrasound treatment group, and the differences were statistically significant ($P < 0.05$). The MRI results showed that, compared with participants in the healthy control group, patients with chronic pain caused by MTrP had decreased AK in the right parahippocampal gyrus, right medial prefrontal cortex, and right inferior frontal gyrus; patients with chronic pain caused by MTrP had decreased MK in the left

Table 6: Brain regions where the MK value of patients with chronic pain caused by MTrP decreased.

Area of interest (AOI)	Peak MNI coordinate			Cluster voxel number	T value
	X	Y	Z		
Left parahippocampal gyrus	−3 3	−21	−14	866	−3.52
Right middle temporal gyrus	55	−58	−15	536	−2.39
Right anterior cingulate cortex	4	46	5	751	−3.81

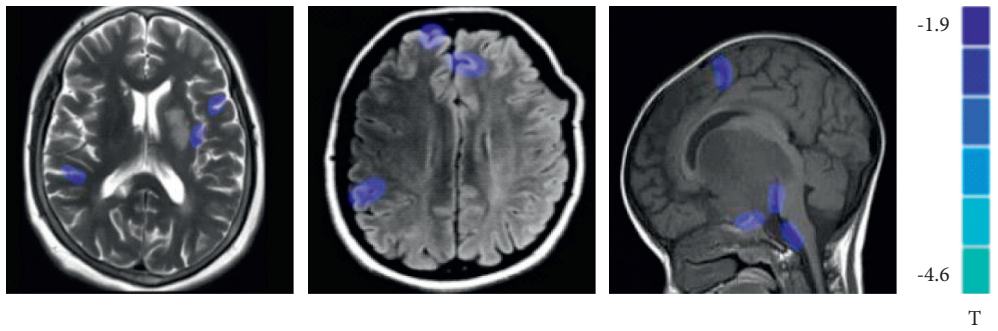

Figure 10: Brain regions where the MK value of patients with chronic pain caused by MTrP decreased. Blue area represented the brain area with reduced MK ($P < 0.05$). The colored bars represented the T value. The left and right side of the figure represented the right and left side of the anatomy, respectively.

Table 7: The brain area where the RK value of patients with chronic pain caused by MTrP decreased.

Area of interest (AOI)	Peak MNI coordinate			Cluster voxel number	T value
	X	Y	Z		
Left lingual gyrus	−13	−58	3	1088	−6.31
Left middle temporal gyrus	−65	−23	−15	899	−5.05
Right precuneus	4	−72	44	430	−2.81

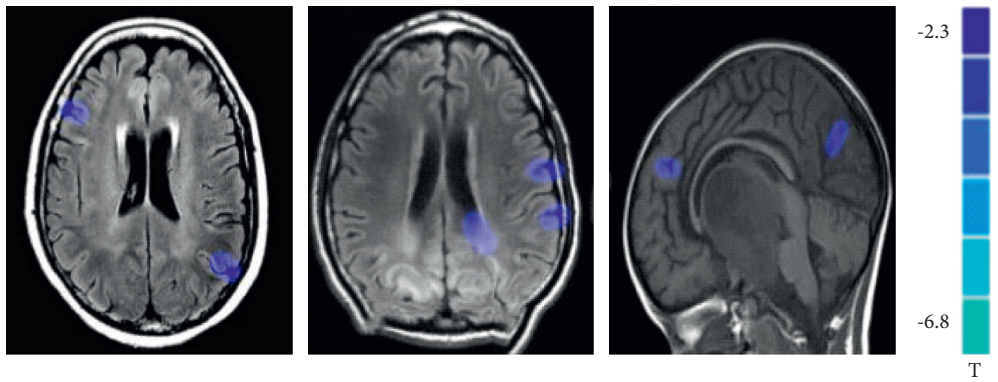

Figure 11: Brain regions where the RK value of patients with chronic pain caused by MTrP decreased. Blue area represented the brain area with reduced RK ($P < 0.05$). The colored bars represented the T value. The left and right side of the figure represented the right and left side of the anatomy, respectively.

parahippocampal gyrus, right middle temporal gyrus, and right anterior cingulate cortex; and the RK of the left lingual gyrus, left middle temporal gyrus, and right precuneus of patients with chronic pain caused by MTrP decrease. Such results were consistent with the research conclusion released by Miller-Patterson C et al. in 2020 [22]. Due to the long-term chronic pain, the gray matter microstructure of the patient's brain has actually changed, and the values of AK, MK, and RK are all decreased in contrast to those of the healthy population to varying degrees. In terms of treatment techniques, the clinical effect of local anesthetic injection therapy was better than ultrasound therapy.

5. Conclusion

In this study, 100 patients with chronic neck pain caused by MTrP were collected. 50 patients were treated with ultrasound and 50 patients were treated with local anesthetic injection. In addition, 50 healthy people were selected as controls. MRI examinations were arranged, and the resulting images were optimized by CNN algorithms. The results showed that, after 3 weeks and 1 month of treatment, the VAS score, PRI score, PPI score, the number of pain days per month, and the number of clinically cured cases in the injection group were better than those of the ultrasound treatment group, and the differences were statistically observable ($P < 0.05$). In addition, the MRI images suggested that, compared with the healthy control group, the brain gray matter microstructure of patients with chronic pain caused by MTrP changed, and the AK, MK, and RK of multiple brain regions were reduced. It revealed that there was indeed a correlation between chronic pain caused by MTrP and central sensitization, and such result may provide new ideas for the treatment of MTrP in the future.

Data Availability

The data used to support the findings of this study are available from the corresponding author upon request.

Conflicts of Interest

The authors declare that they have no conflicts of interest.

References

[1] T. Perreault, J. Dunning, and R. Butts, "The local twitch response during trigger point dry needling: is it necessary for successful outcomes?" *Journal of Bodywork and Movement Therapies*, vol. 21, no. 4, pp. 940–947, 2017.

[2] F. Jin, Y. Guo, Z. Wang et al., "The pathophysiological nature of sarcomeres in trigger points in patients with myofascial pain syndrome: a preliminary study," *European Journal of Pain*, vol. 24, no. 10, pp. 1968–1978, 2020.

[3] X. Gao and J. Cai, "Optimization analysis of urban function regional planning based on big data and GIS technology," *Boletin Tecnico/Technical Bulletin*, vol. 55, no. 11, pp. 344–351, 2017.

[4] A. Galasso, I. Urits, D. An et al., "A comprehensive review of the treatment and management of myofascial pain syndrome," *Current Pain and Headache Reports*, vol. 24, no. 8, p. 43, 2020.

[5] S. Ay, H. E. Konak, D. Evcik, and S. Kibar, "The effectiveness of Kinesio Taping on pain and disability in cervical myofascial pain syndrome," *Revista Brasileira de Reumatologia*, vol. 57, no. 2, pp. 93–99, 2017.

[6] M. McAvoy, J. K. Tsosie, K. N. Vyas et al., "Flexible multielectrode array for skeletal muscle conditioning, acetylcholine receptor stabilization and epimysial recording after critical peripheral nerve injury," *Theranostics*, vol. 9, no. 23, pp. 7099–7107, 2019.

[7] C. Guo, J. Lu, Z. Tian, W. Guo, and A. Darvishan, "Optimization of critical parameters of PEM fuel cell using TLBO-DE based on Elman neural network," *Energy Conversion and Management*, vol. 183, no. MAR., pp. 149–158, 2019.

[8] T. Li, L. Liu, and X. Wang, "[Sepsis impairs aggregation of nicotinic acetylcholine receptors on murine skeletal muscle cell membranes by inhibiting AKT/GSK3β phosphorylation]," *Nan Fang Yi Ke Da Xue Xue Bao*, vol. 39, no. 11, pp. 1337–1343, 2019.

[9] S.-X. Chen, S.-K. Wang, P.-W. Yao et al., "Early CALP2 expression and microglial activation are potential inducers of spinal IL-6 up-regulation and bilateral pain following motor nerve injury," *Journal of Neurochemistry*, vol. 145, no. 2, pp. 154–169, 2018.

[10] L. Madaro, M. Passafaro, D. Sala et al., "Denervation-activated STAT3-IL-6 signalling in fibro-adipogenic progenitors promotes myofibres atrophy and fibrosis," *Nature Cell Biology*, vol. 20, no. 8, pp. 917–927, 2018.

[11] Y. Wang, W. L. Zhai, and Y. W. Yang, "Association between NDRG2/IL-6/STAT3 signaling pathway and diabetic retinopathy in rats," *European Review for Medical and Pharmacological Sciences*, vol. 24, no. 7, pp. 3476–3484, 2020.

[12] H. Chandarana, H. Wang, R. H. N. Tijssen, and I. J. Das, "Emerging role of MRI in radiation therapy," *Journal of Magnetic Resonance Imaging*, vol. 48, no. 6, pp. 1468–1478, 2018.

[13] M. Inglese and M. Petracca, "MRI in multiple sclerosis," *Current Opinion in Neurology*, vol. 31, no. 3, pp. 249–255, 2018.

[14] Z. Lv and W. Xiu, "Interaction of edge-cloud computing based on SDN and NFV for next generation IoT," *IEEE Internet of Things Journal*, vol. 7, no. 7, pp. 5706–5712, 2020.

[15] X. Yang, N. Wang, B. Song, and X. Gao, "BoSR: a CNN-based aurora image retrieval method," *Neural Networks*, vol. 116, pp. 188–197, 2019.

[16] J. Z. Srbely, D. Kumbhare, and L. Grosman-Rimon, "A narrative review of new trends in the diagnosis of MTrP: diagnostic ultrasound imaging and biomarkers," *Journal of the Canadian Chiropractic Association*, vol. 60, no. 3, pp. 220–225, 2016.

[17] V. Evans, M. Behr, A. Gangwar, M. D. Noseworthy, and D. Kumbhare, "Potential role of MRI imaging for myofascial pain: a scoping review for the clinicians and theoretical considerations," *Journal of Pain Research*, vol. 14, pp. 1505–1514, 2021.

[18] E. Cerezo-Téllez, M. Torres-Lacomba, O. Mayoral-Del Moral, B. Sánchez-Sánchez, J. Dommerholt, and C. Gutiérrez-Ortega, "Prevalence of myofascial pain syndrome in chronic nonspecific neck pain: a population-based cross-sectional descriptive study," *Pain Medicine*, vol. 17, no. 12, pp. 2369–2377, 2016.

[19] I. Urits, K. Charipova, K. Gress et al., "Treatment and management of myofascial pain syndrome," *Best Practice & Research Clinical Anaesthesiology*, vol. 34, no. 3, pp. 427–448, 2020.

[20] L. Liu, Q.-M. Huang, Q.-G. Liu et al., "Evidence for dry needling in the management of myofascial trigger points associated with low back pain: a systematic review and meta-analysis," *Archives of Physical Medicine and Rehabilitation*, vol. 99, no. 1, pp. 144–152, 2018, e2.

[21] M. Mardani, E. Gong, J. Y. Cheng et al., "Deep generative adversarial neural networks for compressive sensing MRI," *IEEE Transactions on Medical Imaging*, vol. 38, no. 1, pp. 167–179, 2019.

[22] C. Miller-Patterson, J. Han, K. Yaffe et al., "Clinical and neuroimaging correlates of progression of mild parkinsonian signs in community-dwelling older adults," *Parkinsonism & Related Disorders*, vol. 75, pp. 85–90, 2020.